Journal of Engineering and Applied Sciences 13 (5): 1239-1245, 2018
ISSN: 1816-949X

The Effect of Heat Treatment Conditions on the Microstructural Characterization, Mechanical Properties and Corrosion Behavior of Super Duplex Stainless Steel Casting

[1]Do Van Quang, [2]Bui Thi Thanh Huyen and [1]Tran Duc Huy
[1]School of Material Science and Engineering,
[2]School of Chemical Engineering, Hanoi University of Science and Technology,
Hanoi City, Vietnam

Abstract: The effect of solution annealing temperature ranging from 1050-1100°C and aging at 480°C on the microstructure, mechanical properties and pitting corrosion resistance of Super Duplex Stainless Steel (SDSS) casting were investigated. Obtained results showed that the content of ferrite phase slightly increased as decreasing of austenite phase. The ε-Cu was observed into incoherent type after solution annealing and coherent type after solution annealing and aging at 480°C. The small particles of the ε-phase dispersed in ferrite matrix increase their hardness and diminish corrosion resistance of ferrite phase. Especially, the little negative hysteresis and high breakdown potentials determined from cyclic potentiodynamic polarization curves of SDSS showed that the high pitting corrosion resistance were obtained for the sample with both annealing and aging. The mechanical properties of the SDSS casting were also investigated such as hardness, micro hardness and impact strength. The value of hardness and impact strength of SDSS casting which were solution annealing at 1100°C and aging at 480°C were 295 HB and 77 J, respectively.

Key words: Super duplex stainless steel, corrosion resistance, quenched aging, casting, diminish, impact

INTRODUCTION

Super Duplex Stainless Steels (SDSS) have a two-phase structure containing ferrite and austenite in almost equal proportions and a pitting corrosion resistance of over 40. These materials show an attractive combination of excellent corrosion resistance and high mechanical properties comparing with either austenitic stainless steels or ferritic stainless steels (Nilsson, 1992; Pettersson *et al*., 2015; Ramkumar *et al*., 2015). They have been widely used oil-gas industry such as offshore platforms in applications that involve pumping of produced water (Kang and Lee, 2013). Due to its high ratio of property to cost, super duplex stainless steels have become an alternative to other higher performance materials such as super austenitic stainless steels and Ni-based alloys and have a about 20 year's very successful applications or experiences in the oil-gas industry (Kang and Lee, 2013; Muthupandi *et al*., 2003).

The production of cast components for centrifugal pumps with wall thicknesses exceeding 125 mm (5 inch) in duplex and SDSS has become a complex task due to the low cooling rates during the solidification process. Precipitation of intermetallic and carbide phases are common and include the sigma phase which appears in the highest proportion, sometimes approaching values of close to 20% (Zhang *et al*., 2016; Labanowski, 2007; Li *et al*., 2015). The impact strength of SDSS falls between the impact strength of austenitic and ferritic cast steels, however, even small amounts of secondary phases which precipitate in duplex cast steels, deteriorate the energy of breaking where the influence of σ phase seems to be the most drastic (Chen *et al*., 2002; Martins and Casteletti, 2009; Lopez *et al*., 1991). However, solution annealing heat treatments followed by water quenching dissolves these precipitates and keeps the alloying elements in solid solutions (Li *et al*., 2014; Chen *et al*., 2002; Martins and Casteletti, 2009). Effects of hardening in Duplex Stainless Steel (DSS) may occur at temperatures ranging from 650-950°C and also below 500°C. At higher temperatures, the strength of the material can be compromised because of the formation of σ phase which severely decreases the ductility, toughness and corrosion resistance (Nilsson, 1992). At temperatures below 500°C ferrite can decompose with maximum kinetic at 475°C, causing a drastic reduction in corrosion resistance, loss in ductility and toughness and a great

Corresponding Author: Do Van Quang, School of Material Science and Engineering, Hanoi University of Science and Technology, Hanoi City, Vietnam

increase in hardness as result of precipitation of α' or G-phase (Rovere *et al*., 2013; Li *et al*., 2014). Studies performed by Mateo *et al*. (1997) indicate that there is a cooperative effect of the formation of G-phase and the formation of α′ by spinodal decomposition. Conversely, the precipitation of the G-phase at 475°C requires a very long time of aging to reach uniformity in the ferritic matrix (Sahu *et al*., 2009). Furthermore, the spinodal decomposition features an effect of hardening more pronounced than the one caused by the formation of the G-phase (Danoix *et al*., 2004).

On the other hand, apart from basic ferrite and austenite forming elements, part of duplex cast steel grades contains also copper. In the austenite, the maximum copper solubility at 1094°C amounts to ~8.5% and reaching the value of ~4% at ambient temperature. The copper solubility in ferrite at 1480°C amounts to ~6.0% and goes down with temperature to ~0.2%, causing precipitation of fine-dispersed ε-Cu phase and related with that increase in its hardness (Kang and Lee, 2013; Dyja and Stradomski, 2007). In the light of studies and literature reports using the effect of aging and precipitation of fine-dispersed ε-Cu phase in the ferrite, the resistance to erosion wears of components made of DSS may be increased (Smuk *et al*., 2004). Results of studies presented in paper (Bana and Mazurkiewicz, 2000) have shown that for massive casts the aging is of little effectiveness and the authors suggest abandoning it because of unnecessary increase in the production cost.

Depending on the copper content and heat treatment, the precipitation of the ε-phase occurs in ferritic austenitic stainless steels. The presence of the ε-phase in ferrite increases the hardness of DSS (Smuk *et al*., 2004). Dispersed inclusions of this phase can influence on the stability of passive film and susceptibility of ferrite to pitting corrosion. This effect has been observed in the case of ferritic and duplex ferritic austenitic stainless steels (Banas and Mazurkiewicz, 2000). Up to now, many works have been done about SDSS. However, a few attentions were paid on the influence of copper to corrosion resistance of SDSS in the synthetic sea water solution (Martins and Casteletti, 2009).

In this study, an attempt is to investigate the effect of the heat treatment conditions on the phase volume fraction, microstructure and mechanical properties on the SDSS casting elements such as pump parts, rotors, guide vanes, pipeline elements, etc. Especially, our work presents the influence of thermal aging at 480°C up to 2 h on the corrosion resistance of SDSS in the synthetic sea water solution environment.

MATERIALS AND METHODS

Experimental procedure: The studied materials were prepared by melting process; the raw materials were melted in a medium-frequency induction furnace and then directly poured into the sand moulds. The chemical compositions of the ingots are shown in Table 1.

The ingots were machined into 20×20×10 mm for microstructure analysis and hardness test. Full-sized V-notched Charpy specimens of dimensions 10×10×55 mm with a 2 mm deep V-notch were used in the test of impact strength. All of samples were annealed at different temperature ranging from 1050-1100°C (1050; 1080 and 1100°C) for 2 h then water quenched. The samples after solution annealing treatment at different temperature were aging at 480°C for 2 h. The annealing temperatures were selected based on the equilibrium phase diagram shown in Fig. 1 which was calculated using Thermo-Calc. Software.

The microscopic analysis of the cast steel in as-cast conditions and after heat treatment, respectively was performed on a Zeiss Axiovert 25 optical microscope. To determine the volumetric fractions of phases in the SDSS,

Table 1: Chemical compositions of SDSS casting (mass %)

Elements	Values
C	0.028
Cr	24.60
Ni	5.670
Mo	3.140
N	0.360
Mn	0.500
Si	0.530
Cu	1.350
P	0.020
S	0.030
Fe	Bal.

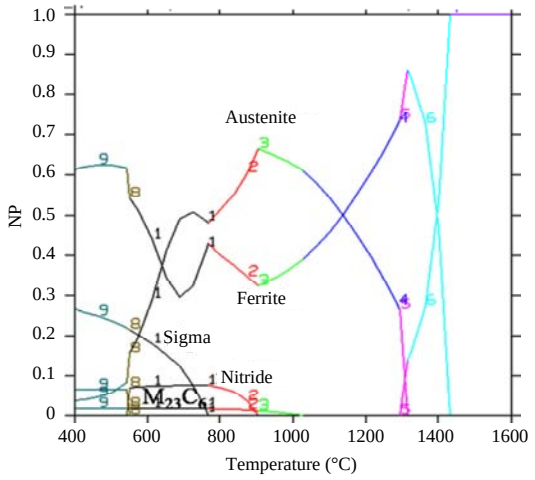

Fig. 1: Phase diagram of super duplex stainless steel

the binary images of the structure were subjected to analysis by Image Pro Plus program. In order to disclose the structure, the cast steel was chemically etched with reagent Mi21Fe (30 g potassium ferricyanide+30 g potassium hydroxide+60 mL distilled water). The structure of ferrite and chemical composition of selected micro-regions were carried out using a Hitachi S-4800 FE-SEM with an EDX microanlyzer.

Cyclic polarization measurements were performed in order to determine the tendency of the alloys to undergo localized corrosion of materials. The cyclic potentiodynamic polarization curves of the alloy were carried out with electrochemical cell by using Autolab PGSTAT 302N (Netherland). The three-electrode system includes of a SDSS working electrode (1 cm^2 surface area), a platinum counter electrode and a Saturated Calomel Electrode (SCE) used as reference electrode. The synthetic sea water was prepared according to the ASTM D 1141 standard as a test solution. To obtain good resolution of the polarization curves, the scanning rate adopted was 5 mV/sec and the immersion time in the open circuit was 1 h prior to initiating the scan.

Hardness was measured by the Brinell method according to the PN-EN ISO 6506-1:2002 standard under a load of 1838 N with a steel ball of a diameter of 2.5 mm. Micro-hardness was measured by the Vickers method on a Duramin-2, micro-hardness tester manufactured by Struers, Denmark. The measurements were taken on metallographic specimens under a load of 0.49 N (HV0.05) and a load action time of 8 sec. Thirty hardness measurements of ferrite and austenite were made for each test. Impact resistance was measured at ambient temperature on a hammer of an initial energy of 300 J.

RESULTS AND DISCUSSION

Figure 2 shows microstructures of the SDSS in as cast condition which were observed using an optical microscope. The optical micrographs present the relatively dark σ phase, bright σ phase (Fig. 2a) and σ phase occurring on the boundary region of the solidification grain (Fig. 2b). The σ phase nucleates most often at the ferrite/austenite interface and grows into the ferrite grains which is promoted both the +higher diffusion rate and by the higher Cr content in ferrite compared to austenite. This phase can be formed also by eutectoid decomposition following the reaction ➔σ+γ' in the temperature range of 700-900°C.

Microstructures of the SDSS depend on solution annealing temperature without aging (Fig. 3) and aging at 480°C (Fig. 4). After solution annealing the cast SDSS is characterized by a diphase ferrite austenite structure. The

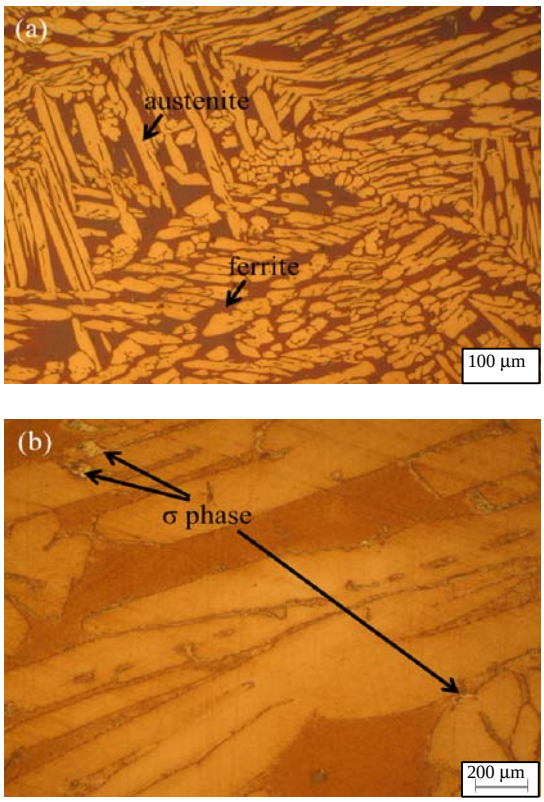

Fig. 2: Optical micrograph of SDSS in as-cast condition: a) Low magnification and b) High magnification

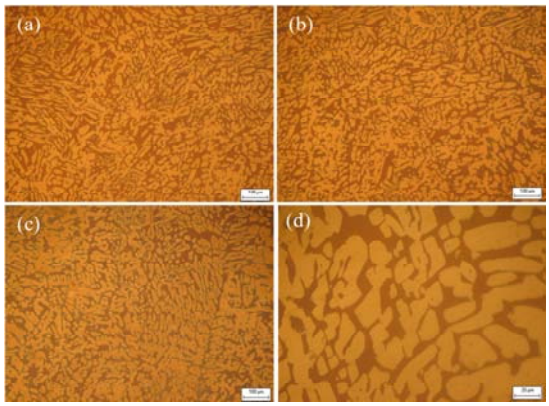

Fig. 3: Optical micrographs of SDSS depend on solution annealing temperature: a) 1050°C; b) 1080°C; c) 1100°C and d) Enlarged image of 1100°C

high temperature of solution annealing provided the dissolution of the σ phase precipitated during cooling after solidification of the cast SDSS from heat samples whereas the high cooling rate prevented its re-precipitation. On the other hand, the volumetric fraction

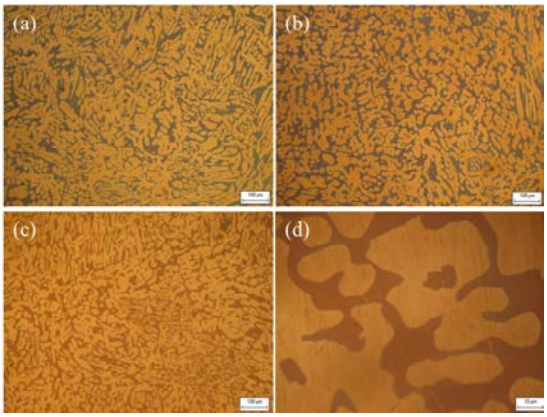

Fig. 4: Optical micrographs of SDSS depend on solution annealing temperature and aging at: a) 480°C; b) 1050°C; c) 1080 °C and d) 1100°C and Enlarged image of 1100°C

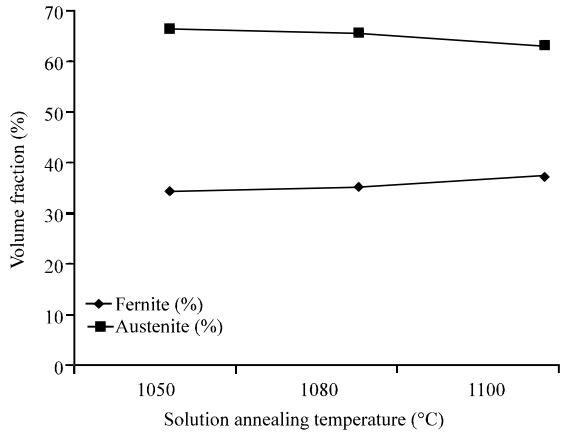

Fig. 5: Volume fraction of ferrite and austenite phases depend on solution annealing temperature

of ferrite phase increased as increasing of solution annealing temperature as showed in Fig. 5. The solution annealing temperature at 1100°C, the volumetric fraction of ferrite and austenite were 37 and 62%, respectively.

The examination results show that, in SDSS casting, the solution annealing temperature in range of 1080-1100°C provides a ferritic austenitic structure of a comparable volumetric fraction of both phases. Water cooling of small specimens as was the case in the laboratory conditions, prevented the precipitation of the σ phase in the structure of the cast SDSS. In industrial conditions, during the solution the heat massive casts at considerably lower and diverse cooling rates an increase in the volumetric fraction of the σ phase and an associated impairment in the properties of the material

Table 2: Hardness, micro-hardness and impact strength depend on solution annealing temperature

Temperature	As-cast	1050°C	1080°C	1100°C
HB	280	260	267	272
HV0.05 δ	302	288	283	285
HV0.05 γ	251	245	251	253
KV (J)	21	89	90	90

Table 3: Hardness, micro-hardness and impact strength depend on solution annealing temperature and aging at 480°C

Temperature	As-cast	1050°C	1080°C	1100°C
HB	280	291	295	295
HV0.05 δ	302	309	318	323
HV0.05 γ	251	270	275	274
KV (J)	21	77	78	77

should be expected. In the SDSS as-cast sample, the impact resistance amounted to 21 J, compared to 90 J obtained for the sample which was heated at 1100°C and water cooling as showing in Table 2.

The copper was used in SDSS to improve the castability and reducing the propensity to porosity, it aims at increasing the frictional properties through aging. The temperature range of precipitation hardening with the ε-Cu phase is 480-510°C (Dyja and Stradomski, 2007; Bana and Mazurkiewicz, 2000).

The FE-SEM examination has shown that before quench aging does not ensure total dissolution of ε-Cu phase precipitating during many hours of massive casts cooling. The lack of characteristic stress contrast around precipitates presented in Fig. 6a shows that they are incoherent. The presence of copper do not dissolved during the solution heat treatment to some extent reduces the effectiveness of subsequent aging. As the result of aging at 480°C was showed in Fig. 6b, uniformly distributed, spherical ε-Cu phase precipitated in ferrite grains and characteristic coffee-bean shape proves their coherence with the matrix. On the other hand, there are many light spherical particles were observed and uniformed distribution on the ferrite matrix; their compositions were confirmed by EDS profiles (Fig. 6c).

Table 2 and 3 show that the overall increase in hardness is determined mainly by the distinct increase in the micro-hardness of ferrite associated with its precipitation hardening, the fine dispersion ε-Cu phase at 480°C. Moreover, causing precipitation of fine-dispersed ε-Cu phase in the ferrite related with that higher hardness of ferrite than austenite. As a result of aging at 480°C (Table 3), uniformly distributed spherical ε-Cu phase precipitated in ferrite grains. Characteristic "coffee-bean" shape proves their coherence with the matrix. Aging at 480°C caused maximum increased in hardness and decline in impact strength as compared with the solution heat treated cast steel (Table 2). On the other hand, it is well

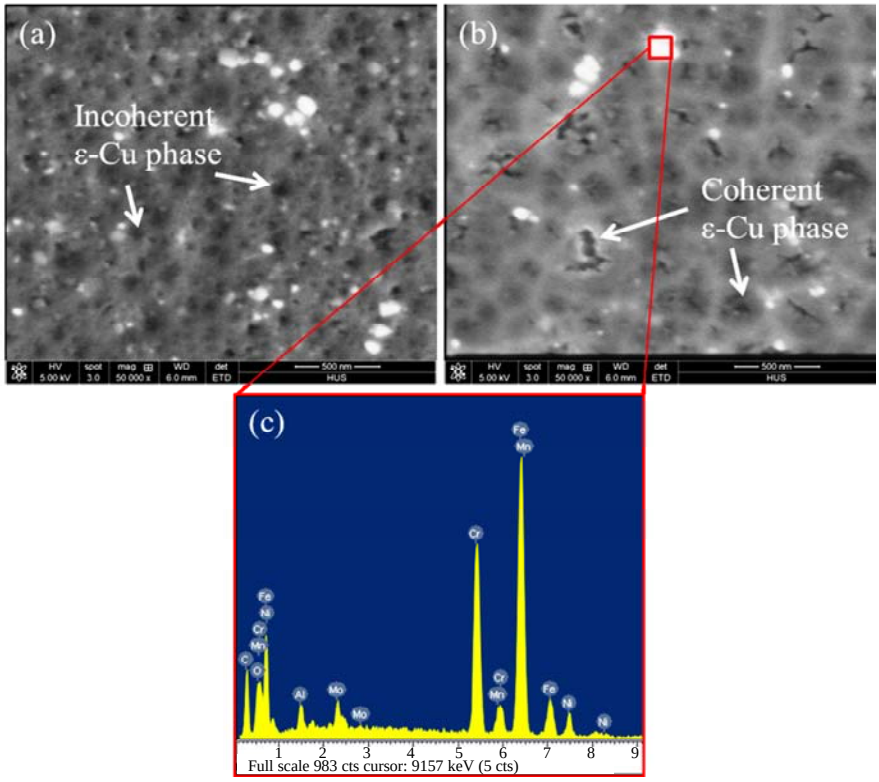

Fig. 6: a) SEM micrographs of solution annealing temperature; b) Aging at 480°C and c) EDS for light spherical particles

known that DSS undergoes '475°C embrittlement' due to a decomposition of ferrite phase into a Cr-rich α′-phase and Fe-rich phase α′-phase in the cast steel aged at 480°C (Rovere *et al*., 2013). This process is accompanied by a strong increase in hardness and decrease in plastic properties. The reduction in cast steel impact strength as a result of spinodal decomposition indicates the necessity to modify the lower aging temperature (Rovere *et al*., 2013; Li *et al*., 2014; Mateo *et al*., 1997).

Cyclic polarization measurements were performed in order to determine the tendency of the alloys to undergo localized (pitting or crevice) corrosion when placed in the electrolyte solutions. The cyclic polarization curves of the samples solution annealed at 1100°C and for the samples treated at the same temperature and then aging at 480°C in the synthetic seawater solution are shown in Fig. 7. Figure 7 shows that, the alloy corroded in the passivation state was due to the presence with a high content of chloride ions in synthetic seawater. Chloride ions cause aqueous corrosion of stainless steels because they increase the electrical conductivity of the solution and penetrate easily into the protective oxide film, thereby breaking its passivity (Martins and Casteletti, 2009). Corrosion potential (E_{corr}), corrosion current density (I_{corr}), pitting corrosion (E_{pit}), re-passivation potential (E_{RP})

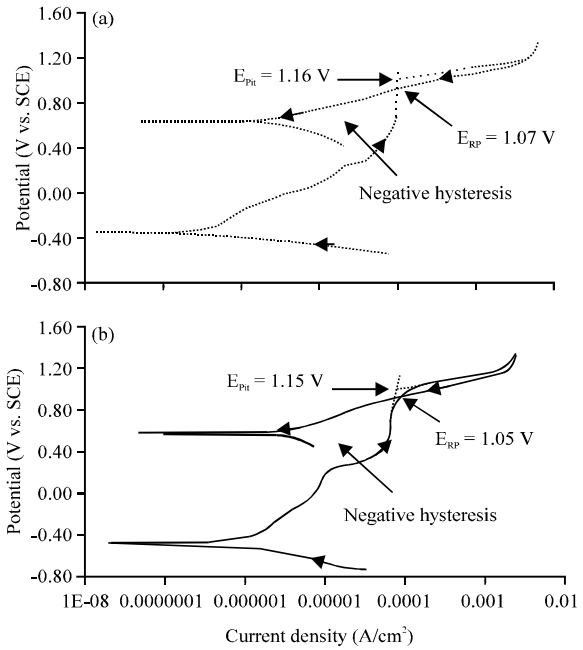

Fig. 7: Anodic cyclic potentiodynamic polarization curves of SDSS after solution annealing at 1100°C without aging: a) Aging at 480°C and b) In the synthetic sea water solution

Table 4: Corrosion parameters extrapolation from cyclic polarization curves of the samples solution annealed at 1100°C with and without aging at 480°C

Samples	Ecorr (V vs. SCE)	Icorr ($\mu A.cm^{-1}$)	Epit (V vs. SCE)	ERP (V vs. SCE)
Without aging	-0.307	0.8	1.16	1.07
Aging at 480°C	-0.430	1.2	1.15	1.05

extrapolated from cyclic polarization curves of the sample solution annealed at 1100°C with and without aging at 480°C are illustrated in Table 4.

Table 4 shows that corrosion current density of the sample after aging at 480°C slightly increase compared with the sample solution annealed at 1100°C. Critical potential for pit formation is represented by (E_{Pit}) which is the potential at which the current density increases very rapidly with a slight change in potential and higher the E_{Pit} greater is the resistance of the material to pit formation (Majumdar *et al*., 2005). The more positive of the E_{RP} value, the higher the corrosion resistance of material (Liang *et al*., 2016). In this study, the material aged at 480°C maintains high values of pitting (1.15 V vs. SCE) and re-passivation (1.05 V vs. SCE) potentials. This means that the aging at 480°C did not cause any detectable damage to the corrosion properties of duplex steel (Park and Kwon, 2002).

Additionally to primary passivation potential and breakdown potential, some quantities that help to understand the corrosion behavior are the curve hysteresis and the repassivation potential (E_{RP}). Differences between the forward and reverse scans result in hysteresis loops. Cyclic polarization curve hysteresis can provide information about corrosion behavior, because positive hysteresis (i.e., the current density during the reverse scan is higher than that for the forward can at any given potential) occurs when the damaged passive film is not repaired and/or pitting is initiated. On the other hand, negative hysteresis (i.e., the current density during the reverse scan is lower than that for the forward scan at any given potential) indicates that the damaged passive film in the both cases (Fig. 7) repair themselves, i.e., high resistance to localized corrosion (Liang *et al*., 2016; Santos *et al*., 2013). Besides, pit growth is not stable on both samples because E_{RP} is larger than E_{corr} (Santos *et al*., 2013). These results indicate that the annealing at 1100°C and then aging at 480°C insignificantly effect on corrosion resistance of the SDSS.

Moreover, the optical micrographs of SDSS after corrosion test which showed in Fig. 8, also, confirmed that many pits were observed on the surface of the sample without aging and aging sample. On the surface of without aging sample, the pits are small and they are located at grain boundaries and inside the ferrite grains

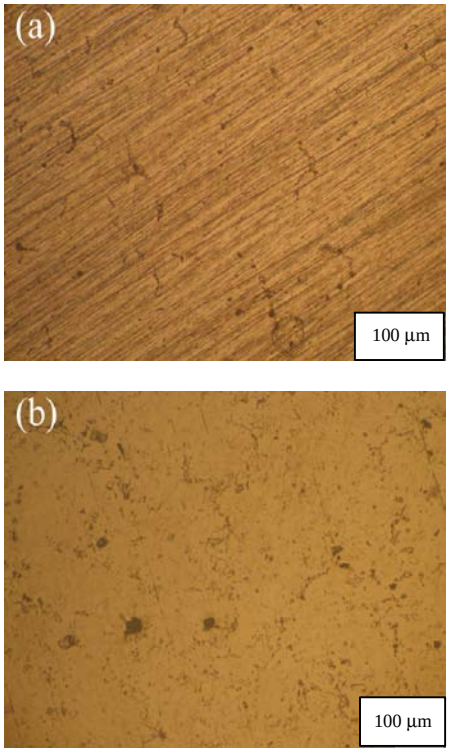

Fig. 8: Optical micrographs of super DSS after corrosion test (without etching): a) Solution annealing temperature at 1100°C and b) Aging at 480°C

(Fig. 8a). After aging, the pits were observed on the sample surface insignificantly increased and larger than without aging case (Fig. 8b). This result is equivalent to corrosion current density shown in Table 4.

CONCLUSION

The heating treatment conditions effect on the microstructure, mechanical properties as well as corrosion resistance of SDSS casting were investigated. After solution heat treatment, the dissolution of the σ phase and completed ferrite-austenite structure were obtained. Especially, ε-Cu phase were observed in a type of incoherent which were solution heat treatment and coherent type which were quench aging at 480°C. The small particles of the ε-phase dispersed in ferrite matrix increase their hardness. Moreover, the material aged at 480°C maintains high values of pitting and re-passivation potentials similar to the annealed sample indicates that the annealing and aging negligibly impact on corrosion behavior and pitting corrosion resistance of the SDSS.

The hardness increased when the samples were quench aging but impact strength decreased compared to solution heat treatment case. The hardness and impact strength values of SDSS casting sample which was solution heat treated at 1100°C and aging at 480°C were 295 HB and 77 J, respectively

ACKNOWLEDGEMENT

This research was supported by T2016-LN-21 Probject which was funded by Hanoi University of Science and Technology.

REFERENCES

Banas, J. and A. Mazurkiewicz, 2000. The effect of copper on passivity and corrosion behaviour of ferritic and ferritic-austenitic stainless steels. Mater. Sci. Eng. A., 277: 183-191.

Chen, T.H., K.L. Weng and J.R. Yang, 2002. The effect of high-temperature exposure on the microstructural stability and toughness property in a 2205 duplex stainless steel. Mater. Sci. Eng. A., 338: 259-270.

Danoix, F., P. Auger and D. Blavette, 2004. Hardening of aged duplex stainless steels by spinodal decomposition. Microsc. Microanal., 10: 349-354.

Dyja, D. and Z. Stradomski, 2007. Quench ageing behavior of duplex cast steel with nano-scale e-Cu particles. J. Achiev. Mater. Manuf. Eng., 20: 435-438.

Kang, D.H. and H.W. Lee, 2013. Study of the correlation between pitting corrosion and the component ratio of the dual phase in duplex stainless steel welds. Corros. Sci., 74: 396-407.

Labanowski, J., 2007. Stress corrosion cracking susceptibility of dissimilar stainless steels welded joints. J. Achiev. Mater. Manuf. Eng., 20: 255-258.

Li, S., Y. Wang and X. Wang, 2015. Effects of ferrite content on the mechanical properties of thermal aged duplex stainless steels. Mater. Sci. Eng. A., 625: 186-193.

Li, S., Y. Wang, X. Wang and F. Xue, 2014. G-phase precipitation in duplex stainless steels after long-term thermal aging: A high-resolution transmission electron microscopy study. J. Nucl. Mater., 452: 382-388.

Liang, H.E., Y.J. Guo, X.Y. Wu, Y.M. Jiang and L.I. Jin, 2016. Effect of solution annealing temperature on pitting behavior of duplex stainless steel 2204 in chloride solutions. J. Iron Steel Res. Intl., 23: 357-363.

Lopez, N., M. Cid and M. Puiggali, 1991. Influence of O-phase on mechanical properties and corrosion resistance of duplex stainless steels. Corros. Sci., 41: 1615-1631.

Majumdar, J.D., A. Pinkerton, Z. Liu, I. Manna and L. Li, 2005. Mechanical and electrochemical properties of multiple-layer diode laser cladding of 316L stainless steel. Appl. Surf. Sci., 247: 373-377.

Martins, M. and L.C. Casteletti, 2009. Microstructural characteristics and corrosion behavior of a super duplex stainless steel casting. Mater. Charact., 60: 150-155.

Mateo, A., L. Llanes, M. Anglada, A. Redjaimia and G. Metauer, 1997. Characterization of the intermetallic G-phase in an AISI 329 duplex stainless steel. J. Mater. Sci., 32: 4533-4540.

Muthupandi, V., P.B. Srinivasan, S.K. Seshadri and S. Sundaresan, 2003. Effect of weld metal chemistry and heat input on the structure and properties of duplex stainless steel welds. Mater. Sci. Eng. A., 358: 9-16.

Nilsson, J.O., 1992. Super duplex stainless steels. Mater. Sci. Technol., 8: 685-700.

Park, C.J. and H.S. Kwon, 2002. Effects of ageing at 475°C on corrosion properties of tungsten-containing duplex stainless steels. Corros. Sci., 44: 2817-2830.

Pettersson, N., S. Wessman, M. Thuvander, P. Hedstrom and J. Odqvist *et al*., 2015. Nanostructure evolution and mechanical property changes during aging of a super duplex stainless steel at 300° C. Mater. Sci. Eng. A., 647: 241-248.

Ramkumar, K.D., A. Singh, S. Raghuvanshi, A. Bajpai and T. Solanki *et al*., 2015. Metallurgical and mechanical characterization of dissimilar welds of austenitic stainless steel and super-duplex stainless steel: A comparative study. J. Manuf. Processes, 19: 212-232.

Rovere, C.A.D., F.S. Santos, R. Silva, C.A.C. Souza and S.E. Kuri, 2013. Influence of long-term low-temperature aging on the microhardness and corrosion properties of duplex stainless steel. Corros. Sci., 68: 84-90.

Sahu, J.K., U. Krupp, R.N. Ghosh and H.J. Christ, 2009. Effect of 475 C embrittlement on the mechanical properties of duplex stainless steel. Mater. Sci. Eng. A., 508: 1-14.

Santos, T.F., R.R. Marinho, M.T. Paes and A.J. Ramirez, 2013. Microstructure evaluation of UNS S32205 duplex stainless steel friction stir welds. Mag. Sch. Mines, 66: 187-191.

Smuk, O., H. Hanninen and J. Liimatainen, 2004. Mechanical and corrosion properties of P/M-HIP super duplex stainless steel after different industrial heat treatments as used for large components. Mater. Sci. Technol., 20: 641-644.

Zhang, Z., H. Jing, L. Xu, Y. Han and L. Zhao, 2016. Investigation on microstructure evolution and properties of duplex stainless steel joint multi-pass welded by using different methods. Mater. Des., 109: 670-685.